J. Med. Chem. 1995, 38, 553–564

Three-Dimensional Structure of Cyclohexapeptides Containing a Phosphinic Bond in Aqueous Solution: A Template for Zinc Metalloprotease Inhibitors. A NMR and Restrained Molecular Dynamics Study

Philippe Cuniasse,† Isabelle Raynal,† Alain Lecoq,† Anasthasios Yiotakis,‡ and Vincent Dive*,†

Département d'Ingénierie et d'Etudes des Protéines D.S.V., CEA, CE Saclay, 91191 Gif sur Yvette Cedex, France, and Department of Organic Chemistry, Laboratory of Organic Chemistry, University of Athens, Panepistimiopolis Zografou, Greece

Received September 22, 1994®

The 3D structures of two phosphinic cyclic hexapeptide inhibitors of bacterial collagenase, cyclo-(Gly^1-Pro^2-Phe$^3\psi$[PO_2-CH_2]Gly^4-Pro^5-Nle^6) (compound **I**) and cyclo(Gly^1-Pro^2-D-Phe$^3\psi$[PO_2-CH_2]-Gly^4-Pro^5-Nle^6) (compound **II**), in aqueous solution, as derived from NMR spectroscopy and molecular dynamics simulations, are described. The general structures of these cyclic hexapeptides closely resemble the "canonic" two-reverse-turn structure, with the proline occupying the (i + 1) position of the turns and the glycine the connecting positions. The phosphinic bond is located between the (i + 2) and (i + 3) positions of one of these turns. However, a striking feature of the backbone structure of these peptides is the presence of double type VIII-turns in compound **I**, and in compound **II** of type VIII- and tentatively named type IX-turns. The comparison of the 3D structures of these two cyclic hexapeptides shows that the stereochemistry of the phenylalanylphosphinyl residue influences not only the local conformation but also the global topology of the peptide macrocycle. The differences in the 3D structure of these compounds are discussed in relation to their inhibitory potencies and with the view of using these constrained cyclic peptides as a scaffold for the development of rigid metalloproteases inhibitors.

Introduction

The number of known proteases containing a zinc atom in their catalytic active sites has rapidly grown in the last few years and will probably continue to increase.[1–4] Analyses of the amino acid sequences of the catalytic domain of these proteases have suggested the existence of different families for these enzymes.[5,6] The determination of the catalytic domain 3D structure for some of these proteases has confirmed this view and unveiled the existence of the "metzincin family".[7–9]

The comparison of the 3D structure of these proteases, belonging to the metzincin family, has further demonstrated the existence of an overall topological equivalence between the catalytic domain of these proteases, a property that probably concerns all the members of this family.[9,10] Moreover, in a subfamily, the active sites of the different members are believed to closely resemble each other.[11,12] Therefore, the specificity of the members in each subfamily should be determined by the existence of very subtle differences between the active site of these closely related proteases. Altogether, these data suggest that it will be a great challenge to discover highly selective inhibitors for the whole zinc protease family. This statement is confirmed by the lack of specificity displayed by some of these members toward synthetic substrates or inhibitors.[13–16]

To overcome this problem, we have initiated a program dealing with the development of both "linear and cyclic" peptide libraries containing a phosphinic bond. Such phosphinic peptides, as analogues of the substrates in the transition state, have been reported to be potent inhibitors of the zinc proteases.[17,18] However, the development of constrained molecules, like the cyclic phosphinic peptides, to achieve a proper selectivity, would certainly take advantage of the precise knowledge of the 3D structure that is stabilized in some of these cyclic pseudopeptides. An important issue in this connection concerns the location and the orientation of the phosphinic bond with respect to the peptide macrocycle. In fact, good interactions between the hydroxyphosphinyl group [PO(OH)] of these cyclic peptides and the zinc atom of the protease active site would be possible only if the hydroxyphosphinyl group is well oriented.

In this paper, the 3D structures in aqueous solution of two cyclic hexapeptides containing a phosphinic bond have been precisely determined by means of NMR and molecular dynamics. These two molecules have been recently shown to be rather potent inhibitors of a bacterial collagenase, an enzyme belonging to the zinc protease family.[19]

Results

1. Conformational Analysis. Due to the presence of the phosphinic group, these two cyclic peptides (compounds **I** and **II**) are highly soluble in water. Therefore, their conformations can be determined using ^{1}H-NMR spectroscopy in this solvent. The 1D proton NMR spectra of compounds **I** and **II** exhibit two sets of resonances in the amide proton region. For both cases, these two sets of resonances, which give rise to negative exchange cross-peaks in the ROESY spectra, must definitely be assigned to cis/trans isomerization of the peptide bonds preceding the two Pro residues. The integration of the resonances in the 1D proton spectra shows for both compounds that the minor component represents less than 10% of the major one. Thus only the major conformer of compounds **I** and **II** will be discussed.

* To whom correspondence should be addressed.
† CEA.
‡ University of Athens.
® Abstract published in *Advance ACS Abstracts*, January 1, 1995.

0022-2623/95/1838-0553$09.00/0

Table 1. ^{1}H-NMR Chemical Shifts of Compounds **I** and **II** in 90% H_2O/10% D_2O at 280 K

	compound **I**	compound **II**
Gly^1 H_N	8.12	7.76
Gly^1 $H_\alpha^{pro\text{-}R}$	3.91	3.56
Gly^1 $H_\alpha^{pro\text{-}S}$	4.21	4.35
Pro^2 H_α	4.12	4.22
Pro^2 $H_\beta^{pro\text{-}S}$	1.92	1.99
Pro^2 $H_\beta^{pro\text{-}R}$	1.09	1.12
Pro^2 $H_\gamma^{pro\text{-}R}$	1.88	1.82
Pro^2 $H_\gamma^{pro\text{-}S}$	1.75	1.82
Pro^2 $H_\delta^{pro\text{-}R}$	3.43	3.35
Pro^2 $H_\delta^{pro\text{-}S}$	3.67	3.52
Phe^3 H_N	7.57	8.33
Phe^3 H_α	4.32	4.26
Phe^3 $H_\beta^{pro\text{-}R}$	2.69	3.22
Phe^3 $H_\beta^{pro\text{-}S}$	3.29	2.74
Phe^3 H_δ	7.31	7.29
Phe^3 H_ϵ	7.35	7.34
Phe^3 H_ζ	7.27	7.26
Gly^4 $H_\alpha^{pro\text{-}S\ a}$	2.81	2.61
Gly^4 $H_\alpha^{pro\text{-}R\ a}$	2.55	2.61
Gly^4 $H_P^{pro\text{-}R}$	1.95	2.24
Gly^4 $H_P^{pro\text{-}S}$	1.58	1.62
Pro^5 H_α	4.37	4.32
Pro^5 $H_\beta^{pro\text{-}S}$	2.37	2.31
Pro^5 $H_\beta^{pro\text{-}R}$	1.96	1.93
Pro^5 $H_\gamma^{pro\text{-}R}$	2.05	2.04
Pro^5 $H_\gamma^{pro\text{-}S}$	2.05	2.04
Pro^5 $H_\delta^{pro\text{-}R}$	3.67	3.60
Pro^5 $H_\delta^{pro\text{-}S}$	3.90	3.75
Nle^6 H_N	8.02	8.24
Nle^6 H_α	4.54	4.43
Nle^6 $H_\beta^{pro\text{-}R}$	1.62	1.60
Nle^6 $H_\beta^{pro\text{-}S}$	1.85	1.88
Nle^6 H_γ	1.25	1.22
Nle^6 H_δ	1.31	1.28
Nle^6 H_ϵ	0.87	0.85

[a] The stereospecific assignment (*pro-R*, *pro-S*) for the pseudo-Gly 4 residue is based on analogy with a standard glycine residue.

Most of the ^{1}H resonances of these two cyclic pseudopeptides (Table 1) can be identified from their coupling patterns (TOCSY experiments, 20 and 80 ms). The assignment of the methylene proton resonances of respectively the phosphinic group (H_{P-C}) and Gly^4 can be unambiguously obtained from the analysis of both the ^{13}C spectra of compounds **I** and **II**, in conjunction with their HMQC spectra. For both hexapeptides, the analysis of the 1D ^{13}C proton-decoupled spectra indicates which carbon is directly attached to the phosphorus atom (Phe^3 C_α and Gly^4 C_P), as their resonances are split due to the P−C coupling (Table 2). This observation, like the analysis of HMQC spectra of these molecules, allows us to assign all the ^{13}C aliphatic resonances of compounds **I** and **II** (Table 3). According to this assignment, the ^{13}C Gly^4 C_P resonance is shifted upfield as compared to the chemical shift of the Gly^4 C_α, an observation expected for a carbon directly bound to a charged hydroxyphosphinyl group. The assignment of the diastereotopic β protons of Phe^3, Nle^6, Pro^2, and Pro^5 residues was carried out by interpretation of the rOe effects and homonuclear vicinal coupling constants. For the two Gly methylenes, as for the hydroxyphosphinyl methylene one (H_{P-C}), a prochiral assignment, consistent with rOe effects, was based on simple geometrical considerations. Observation of rOe's between the Pro^{2,5} H_δ and Gly^{1,4} H_α protons was used to infer that the trans orientation of the peptide bonds preceding the Pro residues is the most highly populated in solution for these cyclic peptides.[20-22] This orientation is confirmed by the characteristic patterns of the $^{13}C_\beta$ and $^{13}C_\gamma$ proline resonances.[23-25]

Table 2. Coupling Constants (Hz) and Temperature Coefficients (ppb/K) of Compounds **I** and **II** in Aqueous Solution at 280 K (Corresponding ϕ values and rotamer populations (%) are reported)

		compound **I**	compound **II**
Gly^1	$^3J(H_N/H_\alpha)^a$	5.7(*pro-R*), 4.8(*pro-S*)	3.2(*pro-R*), 7.4(*pro-S*)
	ϕ calcd^b	-175 ± 10	158 ± 10
		72 ± 10	
	$-\Delta\delta/\Delta T$	4.9	4.8
Phe^3	$^3J(H_N/H_\alpha)^a$	10.3	10.2
	ϕ calcd^c	−106	104
		−134	135
	$^3J(H_N/P)^d$	<0.8	<0.8
	$^3J(H_\alpha/H_\beta^{pro\text{-}R})^a$	13.2	2.9
	$^3J(H_\alpha/H_\beta^{pro\text{-}S})^a$	3.2	13.3
	$\chi_1 = -60°\ ^e$	93	0
	$\chi_1 = 180°\ ^e$	7	5
	$\chi_1 = 60°\ ^e$	0	95
	$^3J(H_\beta^{pro\text{-}R}/P)^d$	6.8	2.5
	$^3J(H_\beta^{pro\text{-}S}/P)^d$	2.0	6.2
	$^1J(C_\alpha/P)^f$	102	111
	$^1J(P/C_P)^f$	92	95
	$-\Delta\delta/\Delta T$	9.3	6.85
Nle^6	$^3J(H_N/H_\alpha)^a$	9.0	8.7
	ϕ calcd^c	−94	−92
		−146	−148
			+60
	$^3J(H_\alpha/H_\beta^{pro\text{-}R})^g$	8.9	8.5
	$^3J(H_\alpha/H_\beta^{pro\text{-}S})^g$	5.8	5.1
	$\chi_1 = -60°\ ^h$	62	58
	$\chi_1 = 180°\ ^h$	29	21
	$\chi_1 = 60°\ ^h$	9	21
	$-\Delta\delta/\Delta T$	2.4	6.3

[a] Determined from the 1D resolution-enhanced ^{1}H-NMR spectra. [b] Possible values for the peptide backbone angle ϕ calculated from ref 38. [c] Possible values for the peptide backbone angle ϕ calculated from ref 39. [d] Determined from the comparison of 1D resolution-enhanced ^{1}H-NMR spectra with and without broadband ^{31}P decoupling. [e] Using the set ^3J_g(H−P) and ^3J_t(H−P) of Siatecki.[33] [f] Determined from ^{13}C-proton-decoupled spectra in hertz. [g] Determined from the DQF-COSY and/or E-COSY spectra. [h] According to Pachler's equations.[60,61]

Table 3. ^{13}C-NMR Chemical Shifts of Compounds **I** and **II** in 90% H_2O/10% D_2O at 280 K

	compound **I**	compound **II**
Gly^1 C_α	45.8	45.1
Pro^2 C_α	65.1	63.3
Pro^2 C_β	32.0	32.0
Pro^2 C_γ	27.2	27.7
Pro^2 C_δ	50.1	50.2
Phe^3 C_α	53.8	52.5
Phe^3 C_β	36.7	35.2
Phe^3 C_γ	140.7	140.2
Phe^3 C_δ	132.4	132.3
Phe^3 C_ϵ	131.4	131.6
Phe^3 C_ζ	129.7	129.7
Gly^4 C_α	28.5	31.0
Gly^4 C_P	25.1	24.7
Pro^5 C_α	64.9	65.1
Pro^5 C_β	32.9	32.7
Pro^5 C_γ	27.6	27.5
Pro^5 C_δ	51.1	50.8
Nle^6 C_α	56.0	56.2
Nle^6 C_β	35.1	33.7
Nle^6 C_γ	30.4	30.4
Nle^6 C_δ	24.7	24.6
Nle^6 C_ϵ	16.2	16.2

Compound I. The chemical shifts for all proton resonances of the cyclic pseudopeptide I in water solution are reported in Table 1. The observation of $^3J(H_N{-}H_\alpha)$ coupling constants larger than 8 Hz for Phe^3 and Nle^6 (Table 2)[26,27] as well as the dispersion of several

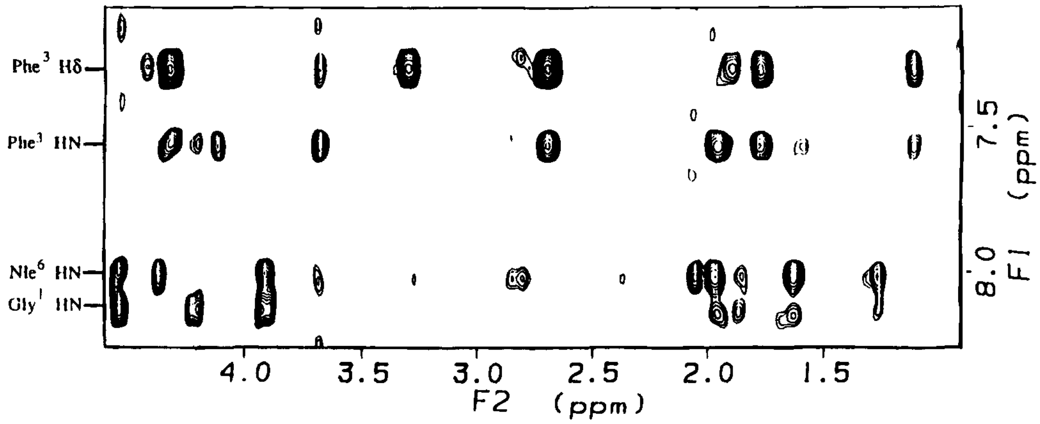

Figure 1. Expanded contour plot of the aromatic NH/aliphatic region of the 165 ms mixing time ROESY spectrum of compound **I** in 90% H_2O/10% D_2O at 280 K.

methylene proton chemical shifts [Gly^1 H_α (0.30 ppm), Gly^4 H_α (0.26 ppm), Gly^4 $H_{P\text{-}C}$ (0.37 ppm), Phe^3 H_β (0.70 ppm), Pro^2 H_β (0.83 ppm)] (Table 1) strongly support the existence of a predominant conformation for this cyclic peptide in aqueous solution.[27-29]

The H_N/$H_{aliphatic}$ region of the ROESY spectrum of compound **I** is reported in Figure 1. Observation of dipolar correlations between the Phe^3 H_N and both the Phe^3 H_α and Pro^2 H_α and between the Nle^6 H_N and both the Pro^5 H_α and Nle^6 H_α protons suggests the presence of a standard two-reverse-turn structure in this peptide, with the Pro^2-Phe^3 and Pro^5-Nle^6 occupying the hinge positions of these turns. Obviously, due to the presence of the phosphinic bond, the Pro^2-Phe^3 reverse turn cannot be stabilized by the classical 4 → 1 hydrogen bond. The folding of the peptide chain around the Pro^2-Phe^3 segment is furthermore inferred from the medium range rOe's between the Phe^3 H_N and Gly^1 $H_\alpha^{pro\text{-}S}$ and the Phe^3 H_N and Gly^4 $H_{P\text{-}C}^{pro\text{-}R}$. At the Pro^5-Nle^6 level, the observation of a Nle^6 H_N− Gly^4 $H_\alpha^{pro\text{-}S}$ rOe connectivity leads to a similar conclusion. Furthermore, the rOe's between Phe^3 H_N−Pro^2 H_δ, Phe^3 H_N−Pro^2 H_γ, and Phe^3 H_N−Pro^2 $H_\beta^{pro\text{-}R}$ show a specific orientation of the peptide bond between the Pro^2 and Phe^3 residues, in which the H_N points up relative to the average ring plane of the peptide macrocycle (peptide chain viewed as running clockwise). The same type of orientation for the peptide bond between Pro^5-Nle^6 is demonstrated by similar rOe's between the Nle^6 H_N and the Pro^5 ring protons (Figure 1). This particular orientation of the peptide bond between the $(i + 1)$ and $(i + 2)$ residues of a turn is that observed in the so-called βI-turn.[30] At the Pro^5−Nle^6 segment level, one of the two possible ϕ values of the Nle 6 residue obtained from quantitative analysis of the $^3J(H_N-H_\alpha)$ coupling constants (−94) (Table 2) fits with the expected ϕ value of the $(i + 2)$ residue in a βI-turn. However, the low-field chemical shift of the Gly^1 H_N resonance (8.12 ppm), like the value of the temperature coefficient of this proton (−4.9 ppb/K), suggests that the Gly^1 H_N proton is not involved in a 4 → 1 hydrogen bond, as generally found for a classical βI-turn. Quantitative analysis of the $^3J(H_\alpha-H_\beta)$ vicinal coupling constants of Nle^6 shows that the rotamer I is predominant (Table 2). This is consistent with the observation of a Nle^6 H_γ−Pro^5 H_β dipolar correlation (not shown).

At the Pro^2-Phe^3 segment level, the ϕ values compatible with the $^3J(H_N-H_\alpha)$ of the Phe^3 residue (Table 2) show that the H_N and H_α protons of this residue are in a trans orientation relative to the N−C_α bond. Taking into account the orientation of the peptide bond between Pro^2 and Phe^3, this observation demonstrates that the Phe^3 residue of compound **I** has L stereochemistry. Further, the preferred orientation of the phenyl side chain is shown by the presence of several rOe's between the aromatic Phe^3 protons and the Pro^2 ring protons (Figure 1). These rOe's imply that the aromatic ring points over the pyrrolidine ring and assume that the phenyl side chain is in a trans orientation with respect to the hydroxyphosphinyl group (the so-called rot. I). According to these observations, the rotamer I population, calculated from the vicinal coupling constants $^3J(H_\alpha-H_\beta)$, is 93% (Table 2). This conformation of the Phe^3 side chain is also consistent with the atypic Pro^2 $H_\beta^{pro\text{-}R}$ chemical shift (1.09 ppm, Table 1), probably due to anisotropy effects of the aromatic ring.[31] Both the configuration of the phenyl side chain and its orientation are furthermore corroborated by the observation of an rOe effect between the Phe^3 H_N and Phe^3 $H_\beta^{pro\text{-}R}$. In fact, such an effect in a type I turn is only possible for an L residue having its side chain in the rot. I orientation.[32] The particular set of $^3J(H_\alpha-H_\beta)$ coupling constants measured for Phe^3 emphasizes that the constraints in this cyclic peptide concern both the backbone and this side chain. It should be noticed that the $^3J(P-H_\beta^{pro\text{-}R})$ and $^3J(P-H_\beta^{pro\text{-}S})$ are respectively 6.8 and 2.0 Hz. Such different values are not expected for a rotamer I, as this conformation places the two H_β protons of residue Phe^3 in the gauche orientation relative to the phosphorus atom. Nevertheless, it should be pointed out that some studies of phosphorus compounds have reported vicinal proton−phosphorus coupling constants of 4.2 Hz, corresponding to a gauche orientation of the proton relative to the phosphorus, and 33 Hz, for the trans orientation.[33] This set of $^3J_g(H-P)$ and $^3J_t(H-P)$ values, which is not necessarily the more appropriate set for a phenylalanylphosphinyl residue, due to the marked difference between ^3J_g and ^3J_t, indicates that a small percentage of the rot. II will be sufficient to produce the observation of different $^3J(H_\beta-P)$ coupling constants, as those reported for the Phe^3 of this peptide. The measurement of a low value for $^3J(H_\beta^{pro\text{-}S}-P)$ (2 Hz) in compound **I** suggests that the $^3J_g(H-P)$ value of 4.3 Hz may not be applicable to our compound. In addition, it should be noticed that the Phe^3 H_N proton resonance does not exhibit coupling with

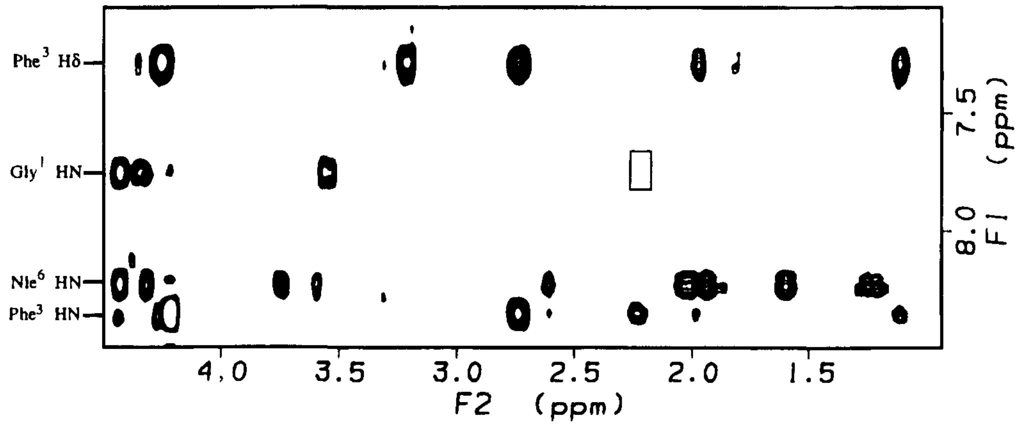

Figure 2. Expanded contour plot of the aromatic NH/aliphatic region of the 165 ms mixing time ROESY spectrum of compound **II** in 90% H_2O/10% D_2O at 280 K. The box indicates the Gly^1H_N–$Gly^4H_P^{pro\text{-}R}$ rOe which does not appear in this figure but is observed at lower levels in this experiment and in ROESY experiments at lower mixing time.

the phosphorus atom ($^3J(H_N-P)$ is at most not greater than 0.8 Hz) (Table 2).

Compound II. This molecule exhibits several NMR parameters–dispersions of both the $^3J(H_N-H_\alpha)$ coupling constants and the methylene proton chemical shifts (Table 1), which are similar to those observed for compound **I**. However, the inversion of the phenyl side chain stereochemistry promotes additional constraints in this cyclic peptide at long distances, as suggested by the large increase in both the chemical shift nonequivalence of Gly^1 ($\Delta H_\alpha, H_\alpha'$) in compound **II** (0.34 ppm in **I** → 0.80 ppm in **II**) and the difference in the values of Gly^1 $^3J(H_N-H_\alpha,H_\alpha')$ (Table 2). The H_N/aliphatic region of the ROESY spectrum of compound **II** is reported in Figure 2. Despite the differences pointed out above between compounds **I** and **II**, the qualitative interpretation of the rOe's indicates the presence of a Pro^5-Nle^6 βI-turn in this part of the molecule. On the other side of the molecule, a strong rOe between Pro^2 H_α and Phe^3 H_N and the lack of Phe^3 H_N–Pro^2 H_δ rOe support the presence of a type II β-turn, as expected for a reverse-turn containing a D amino acid residue in the $(i + 2)$ position. The observation of a Phe^3 H_α–Gly^4 $H_\alpha^{pro\text{-}R}$ rOe (not shown), not observed in compound **I**, is consistent with a D stereochemistry of the Phe^3 residue. Indeed, in this stereochemistry, the Phe^3 H_α points on the same side of the peptide macrocycle as the Gly^4 H_α protons, thus explaining this rOe. In this molecule, rOe's are also observed between the Phe^3 aromatic protons and the proline ring protons, indicating a rotamer I conformation for this side chain. The rotamer I population, calculated from the $^3J(H_\alpha-H_\beta)$ values, is 95% (Table 2). The remarks made above for compound **I**, regarding the $^3J(H_\beta^{pro\text{-}R}-P)$ and $^3J(H_\beta^{pro\text{-}S}-P)$ values (respectively 2.5 and 6.2 Hz), could also be applied to compound **II**. As already noted for compound **I**, the NH proton resonance of Phe^3 in this compound does not exhibit coupling with the phosphorus atom (Table 2).

2. Conformations Generated from NMR Restraints. To define the solution conformation of both pseudohexapeptides, a set of respectively 26 and 20 distance restraints for compounds **I** and **II** has been determined from the analysis of ROESY experiments (Table 4), as reported in the Experimental Section. These distances were used to generate a set of 100 structures for each compound with the procedure of simulated annealing described in the Experimental Section. The $^3J(H_N-H_\alpha)$ coupling constants have not been used as distance restraints in this procedure, but instead the consistency of these coupling constants with the resulting structures has been checked and used to select the most probable conformations. The conformations of the Phe^3 and Nle^6 side chains have been constrained to the most populated rotamers, as determined from analysis of rOe effects and homonuclear $^3J(H_\alpha-H_\beta)$ vicinal coupling constants. When observed, the side chain–side chain rOe's from Phe^3 to Pro^2, and also from Nle^6 to Pro^5 (Table 4), have not been used as input constraints for several reasons. First, the calibration of the side chain–side chain rOe's, using backbone rOe, may introduce appreciable errors in the resulting distances due to different dynamic behaviors of these protons, as compared to the pair of protons taken as reference. Second, rOe's which involve side chain protons may be influenced by the population of rotamers.[34] However, the consistancy of all the side chain–side chain rOes have been checked in the final structures. In the case of the Phe^3 aromatic protons, the assignment of these resonances were made using both HMQC[35] and HMBC[36] experiments. Thus the Phe^3 aromatic protons which give rOe's with the pyrolidine ring protons of the Pro^2 residue were assigned to the Phe^3 H_δ protons.

Compound I. Analysis of the data reported in Table 4 shows that the generated structures reproduce quite well the experimental distance restraints, since no distance restraint violation higher than 0.1 Å is observed in the set (considering the uncertainty used in the distance restraints). The mean rmsd on the distance violations for the structures set is 0.033 Å. This shows that the NMR data set is consistent and confirms the existence of essentially one conformation in aqueous solution. The mean ϕ and ψ angles in the 100 structures generated calculated for each residue are reported in Table 5. The corresponding rmsd values are remarkably low (less than 3.5°) indicating that the conformational space compatible with the NMR restraints is extremely limited, even using a large uncertainty in the distance restraints (±20%). The small values of the rmsd on the ϕ and ψ angles show that the 100 structures belong to the same conformational family.

Thus, Figure 3 shows one of the structures generated for compound **I** which is representative of the unique conformational family. The conformation obtained is a

Table 4. Comparison of Experimental and Calculated Proton–Proton Distances of Compounds **I** and **II**

	I			**II**		
protons	ROESY*	SA*	TAMD*	ROESY*	SA*	TAMD*
Gly^1 H$_N$–Nle^6 H$_N$				2.60	2.72	2.88
Gly^1 H$_N$–Gly^1 H$_\alpha^{pro\text{-}R}$	2.60	2.75	2.62	2.70	2.55	2.54
Gly^1 H$_N$–Gly^1 H$_\alpha^{pro\text{-}S}$	2.60	2.76	2.73	2.70	2.92	2.69
Gly^1 H$_N$–Nle^6 H$_\alpha$	2.30	2.43	2.38	2.35	2.70	2.45
Gly^1 H$_N$–Gly^4 H$_P^{pro\text{-}R}$	3.50	3.64	3.60	3.70	4.45	3.83
Gly^1 H$_\alpha^{pro\text{-}S}$–Pro^2 H$_\delta^{pro\text{-}S}$	2.10	2.35	2.39	ND		
Gly^1 H$_\alpha^{pro\text{-}S}$–Pro^2 H$_\delta^{pro\text{-}R}$	2.50	3.00	2.69	2.30	2.78	2.35
Gly^1 H$_\alpha^{pro\text{-}R}$–Pro^2 H$_\delta^{pro\text{-}R}$	2.20	2.40	2.41	ND		
Phe^3 H$_N$–Gly^1 H$_\alpha^{pro\text{-}S}$	3.30	3.70	3.42			
Phe^3 H$_N$–Pro^2 H$_\alpha$	3.10	3.62	3.40	1.90	2.23	2.17
Phe^3 H$_N$–Pro^2 H$_\delta^{pro\text{-}S}$	2.80	2.61	2.67			
Phe^3 H$_N$–Pro^2 H$_\gamma^{pro\text{-}S}$	2.90	2.38	2.94			
Phe^3 H$_N$–Pro^2 H$_\beta^{pro\text{-}R}$	3.40	3.55	3.36	3.90	3.50	3.65
Phe^3 H$_N$–Phe^3 H$_\alpha$	2.60	2.93	2.77	2.95	2.89	2.91
Phe^3 H$_N$–Gly^4 H$_P^{pro\text{-}S}$	3.70	4.04	3.59			
Phe^3 H$_N$–Gly^4 H$_P^{pro\text{-}R}$	2.70	2.90	2.78	3.10	2.48	3.05
Phe^3 H$_\alpha$–Gly^4 H$_P^{pro\text{-}S}$	2.50	2.85	2.72			
Phe^3 H$_\alpha$–Gly^4 H$_P^{pro\text{-}R}$				2.70	3.27	2.81
Phe^3 H$_\alpha$–Gly^4 H$_\alpha$				2.30[a]	2.76[a]	3.41[a]
Phe^3 Ar–Phe^3 H$_\alpha$	2.55[b]	2.90[c]	2.83[c]	2.80[b]	2.92[c]	2.99[c]
Phe^3 Ar–Phe^3 H$_\beta^{pro\text{-}S}$	2.80[b]	2.84[c]	2.77[c]	2.80[b]	2.62[c]	2.69[c]
Phe^3 Ar–Phe^3 H$_\beta^{pro\text{-}R}$	2.60[b]	2.62[c]	2.62[c]	2.90[b]	2.85[c]	2.85[c]
Phe^3 Ar–Pro^2 H$_\alpha$				3.60[b]	5.38[c]	4.89[c]
Phe^3 Ar–Pro^2 H$_\beta^{pro\text{-}S}$				3.85[b]	5.61[c]	5.48[c]
Phe^3 Ar–Pro^2 H$_\beta^{pro\text{-}R}$	3.30[b]	3.66[c]	3.67[c]	3.60[b]	3.80[c]	2.85[c]
Phe^3 Ar–Pro^2 H$_\gamma^{pro\text{-}R}$	3.65[b]	4.57[c]	5.29[c]			
Phe^3 Ar–Pro^2 H$_\gamma^{pro\text{-}S}$	3.15[b]	3.00[c]	3.62[c]			
Phe^3 Ar–Pro^2 H$_\delta^{pro\text{-}S}$	4.05[b]	5.34[c]	4.78[c]			
Gly^4 H$_\alpha^{pro\text{-}S}$–Gly^4 H$_P^{pro\text{-}R}$	2.60	2.44	2.58			
Gly^4 H$_\alpha^{pro\text{-}R}$–Gly^4 H$_P^{pro\text{-}S}$	2.40	2.40	2.36	2.60[a]	2.70[a]	2.74[a]
Gly^4 H$_\alpha^{pro\text{-}S}$–Pro^5 H$_\delta^{pro\text{-}S}$	2.10	2.51	2.33	2.30[a]	2.61[a]	2.80[a]
Gly^4 H$_\alpha^{pro\text{-}S}$–Pro^5 H$_\delta^{pro\text{-}R}$	2.30	2.68	2.54	2.30[a]	2.52[a]	2.72[a]
Gly^4 H$_\alpha^{pro\text{-}R}$–Pro^5 H$_\delta^{pro\text{-}R}$	2.40	2.33	2.55			
Nle^6 H$_N$–Gly^4 H$_\alpha^{pro\text{-}S}$	3.40	3.83	3.59	3.30[a]	3.98[a]	4.22[a]
Nle^6 H$_N$–Pro^5 H$_\alpha$	2.90	3.54	3.23	2.75	3.41	2.69
Nle^6 H$_N$–Pro^5 H$_\delta^{pro\text{-}S}$	2.60	2.73	2.67	2.85	2.69	3.29
Nle^6 H$_N$–Pro^5 H$_\beta^{pro\text{-}R}$	2.90	2.38	3.00	2.90	3.50	2.80
Nle^6 H$_N$–Pro^5 H$_\gamma^{pro\text{-}R}$				2.90	2.45	3.25
Nle^6 H$_N$–Nle^6 H$_\alpha$	2.50	2.95	2.76	2.40	2.92	2.32

[a] Restraints corresponding to $<r^{-6}>$ of both *pro-R* and *pro-S* protons due to resonance overlap. [b] Not used as input restraints for reasons discussed in the text. [c] Restraints corresponding to $<r^{-6}>$ of both Phe H$_{\delta 1}$ and Phe H$_{\delta 2}$ protons. *: ROESY, NMR-derived distances; SA, distances obtained in the simulated annealing structures; TAMD, distances obtained from the time-averaged molecular dynamics. ND: not determined due to resonance overlap.

Table 5. Mean ϕ and ψ Values of Compounds **I** and **II**, as Obtained from the Simulated Annealing Procedure (Corresponding rmsd's are reported in brackets)

	Gly^1	Pro^2	Phe^3	Gly^4	Pro^5	Nle^6
compound **I**						
ϕ	−178 (1.9)	−82 (0.1)	−131 (0.2)	176 (0.4)	−70 (3.5)	−130 (1.7)
ψ	−176 (0.7)	−34 (0.4)	64 (0.6)	−160 (1.0)	−53 (0.7)	74 (2.3)
compound **II**						
1[a] ϕ	108 (1.0)	−83 (0.1)	133 (0.1)	177 (0.5)	−81 (0.1)	−118 (1.1)
ψ	−103 (0.9)	129 (0.3)	−59 (0.1)	−179 (0.4)	−31 (0.1)	42 (3.3)
2[a] ϕ	148 (1.6)	−81 (0.1)	139 (0.1)	−172 (0.1)	−81 (0.1)	−143 (0.8)
ψ	−157 (0.1)	136 (0.3)	−56 (0.1)	174 (0.5)	−33 (0.2)	54 (2.6)

[a] The ϕ and ψ values of the two conformations obtained from the SA procedure are reported.

two-reverse-turn type, the proline residues being at the $(i + 1)$ position of the turns. In this structure, the resulting ϕ and ψ Pro^2 and Pro^5 values correspond approximately to the values reported for a type I turn.[37] In contrast, both the ϕ and ψ Phe^3 and Nle^6 values are outside of the range of the ϕ and ψ values generally observed for the $(i + 2)$ residue in a βI-turn. Among the different restraints in this cyclic peptide, which can be responsible for these particular ϕ and ψ values of the $(i + 2)$ residue, at least for the Nle^6, the large rOe observed between Nle^6 H$_\alpha$ and Gly^1 H$_N$ (Figure 1) should contribute significantly to the ψ value of Nle^6. Indeed, only a ψ Nle^6 value around 70° places the Gly^1 H$_N$ and Nle^6 H$_\alpha$ protons at a short distance. It should be noticed that the rOe between the Gly^1 H$_N$ and Nle^6 H$_N$ has not been used as distance restraint because the distortion of the base-plane near the diagonal peaks leads to uncertainty in the integration of the corresponding cross-peaks in the ROESY experiments. The presence of this correlation has been checked using a "soft" ROESY experiment (not shown). Unfortunately, in this experiment, the calibration of the distance was not possible. However, the weakness of this correlation in the "soft-" ROESY, as in the standard ROESY experiments, is consistent with the corresponding distance measured in the structures obtained for compound **I** (3.8 Å). Further, the shift of the ψ Nle^6 value at 74°, which implies a perpendicular orientation of the peptide bond

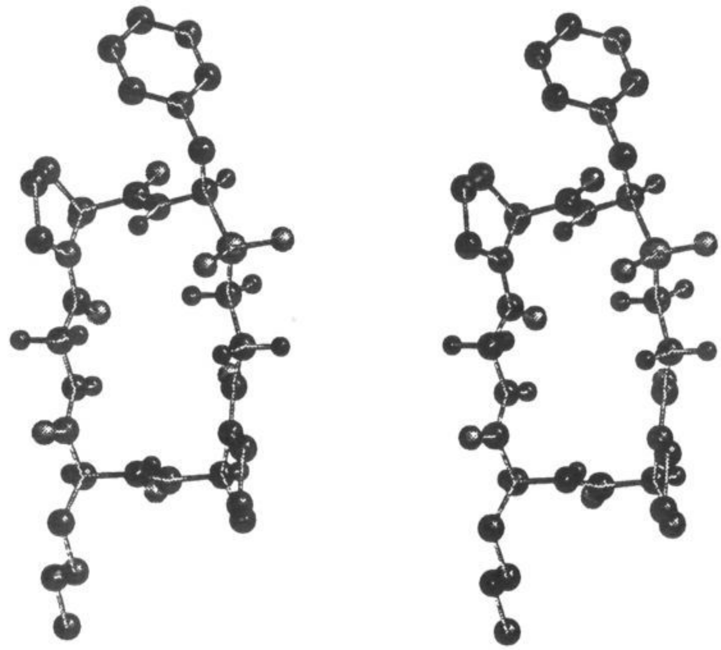

Figure 3. Stereoview of one of the structures generated for compound **I** obtained by the SA procedure. This structure is representative of the unique conformational family obtained for compound **I** (see Table 5 which gives the mean ϕ and ψ values and the corresponding rmsd for these structures). For side chains, the protons bound to carbons are not shown.

between the Nle^6 and Gly^1 residues with respect to the peptide macrocycle, might explain why the Gly^1 H_N does not appear as hydrogen-bonded in this cyclic peptide. The ϕ values of Gly^1, Phe^3, and Nle^6 (−178°, −130°, and −131°) reproduce reasonably well the experimental ϕ values deduced from the experimental $^3J(H_N-H_\alpha)$ coupling constants.[38,39] The H−N−C−P angle in the phosphinic residue measured in the final structure of compound **I** is 50°. As already noted in the result section, the $^3J(H_N-P)$ of the phosphinic residue is less than 0.8 Hz. Even though no Karplus relation for $^3J(H_N-P)$, as a function of the H−N−C−P dihedral angle, is available in the literature for this type of residue, it can be noted that in the Karplus relation calibrated for $^3J(P-H)$, as a function of the P−O−C−H dihedral angle, a value around 1 Hz corresponds to a torsion angle of 60°.[40]

According to the nomenclature proposed by Wilmot and Thornton,[37] the two reverse turns, as observed in this cyclic peptide, with the particular ϕ,ψ values of the $(i + 2)$ residues (Phe^3, Nle^6), should be described as belonging to the type VIII-turn category. In fact, the typical ϕ,ψ values reported for the $(i + 1)$ and $(i + 2)$ residues in this turn are respectively −60°, −30° and −120°, 120°. These β-turns are characterized by a significant deviation of the $\psi(i + 2)$ value from zero toward the positive values, corresponding to the β region of the Ramachandran map.[37]

Compound II. The 100 structures generated with the SA procedure for compound **II** can be separated into two different conformations (conformations 1 and 2 in Table 5). These two conformations exhibit identical ϕ,ψ values for Pro^2 to Pro^5 residues but differ from each other by the ϕ,ψ values of residues Gly^1 and Nle^6 (Table 5). Indeed, the first conformation gives a ϕ,ψ set of 108°, −103°) for Gly^1 and a ϕ,ψ set of −118°, 42° for Nle^6, while the second conformation gives a set of 148°, −157° for the Gly 1 residue and −143°, 54°) for the Nle 6 residue. The corresponding rmsd for the ϕ,ψ values are very low (less than 3.3°) in each family. For the Gly^1 residue, these two possible sets of ϕ,ψ are probably related to the fact that, for chemical shift degeneracy reasons, no distance constraints have been used between the Pro^5 H_δ and Gly^4 H_α. However, taking into account the unusual dispersion in the chemical shift displayed by the Gly^1 $H_\alpha,H_{\alpha'}$, a local mobility of the Gly^1 residue appears unlikely. Further, the $^3J(H_N-H_\alpha)$ coupling constant measured for the Gly^1 (3.2−7.4 Hz) is consistent only with the ϕ value of 148° (Table 2). These arguments suggest that the conformation with the ϕ value of 148° for the Gly^1 is probably the one present in solution. The ϕ Nle^6 angle of this latter conformation (−143°) is furthermore in better agreement with the $^3J(H_N-H_\alpha)$ observed for this residue (8.7 Hz) ($\phi = -118°$ should correspond to a value of 11 Hz for the corresponding $^3J(H_N-H_\alpha)$. As shown in Table 5, the rmsd on the ϕ and ψ angles are very low for family 2. Thus one of the structures of the selected conformation 2 for compound **II** is shown in Figure 4. In this structure, on the basis of the ϕ,ψ values of the $(i + 1)$ and $(i + 2)$ residues, the Gly^4-Pro^5-Nle^6-Gly^1 segment adopts a type VIII-turn, as observed for compound **I**.[37] In the Gly^1-Pro^2-Phe^3-Gly^4 region, due to the presence of a D-Phe, the ψ Pro^2 and ϕ,ψ Phe^3 values are different from those observed in I for the same residues. In this region, one major conformational difference between compounds **I** and **II** concerns the orientation of the peptidic plane between Pro^2 and Phe^3 and the value of ψ Phe^3. The ϕ,ψ values observed for D-Phe^3 (139°, −56°) are different from those reported for a type II β-turn. However, this topological difference between compounds **I** and **II** is similar to that existing between type I and type II β-turns. Thus on the basis of this analogy, we propose to call the reverse turn present in the Gly^1-Pro^2-Phe^3-Gly^4 region a type IX-turn.

3. MD Simulations with Time-Dependent Distance Restraints. A closer look at Table 4 reveals that the major inconsistency between the experimental and

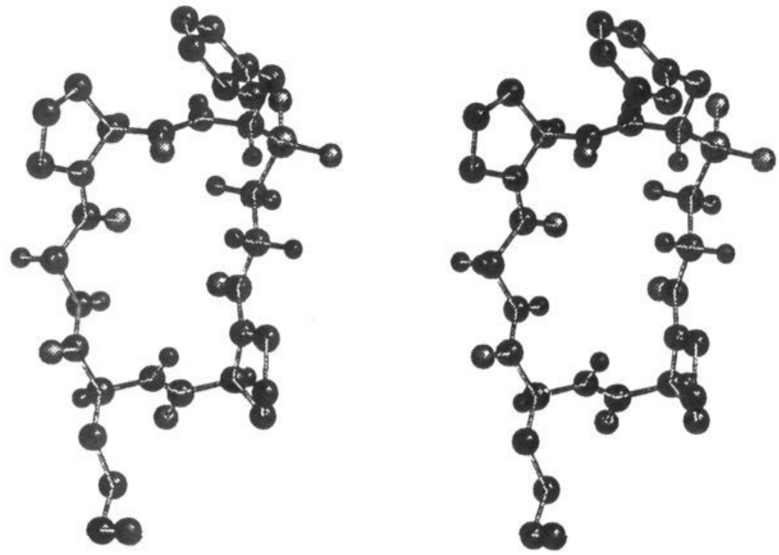

Figure 4. Stereoview of the selected structure of compound **II** obtained from the SA procedure. This structure is representative of the selected conformational family 2 obtained for compound **II** (see Table 5 in which are reported the mean ϕ and ψ values and the corresponding rmsd). For side chains, the protons bound to carbons are not shown.

calculated distances in compound **I** involves the Phe^3 H_N and Nle6 H_N, the two amide protons located on the peptide bond occupying the hinge position of the reverse turns in this peptide. Several conformational analyses of cyclic penta- and hexapeptides have shown the occurrence of a conformational equilibrium in these cyclic peptides, involving mainly the orientation of the peptide bond at the hinge position.[32,34,41-43] Two stable orientations of this peptide bond have been generally observed, in which the amide group of the peptide bond points up (as in a type βI-turn) or down (as in a type βII-turn) relative to the average ring plane of the macrocycle (peptide chain viewed as running clockwise).[41] Furthermore, these two conformations of the central peptide bond have been proposed to be in rapid exchange on the NMR time scale, and the population of the two conformers can be approximated from the experimental distance determined between the $H_N(i + 2)$ and $H_\alpha(i + 1)$ protons.[41] In the case where only one conformer occurs, the reference distance between these two protons is 3.5 Å when the H_N points up or 2.1 Å when the H_N points down.[41,44] For compound **I**, the experimental Phe^3 H_N−Pro^2 H_α distance of 3.1 Å indicates that 95% of the conformers have the Phe^3H_N pointing up, while the 2.9 Å distance between Nle^6 H_N and Pro^5 H_α leads to a population of 90% for the orientation of this peptide bond. The same calculation for compound **II** shows that the peptide bond between Pro^2 and Phe^3 adopts only one orientation, the H_N pointing down relative to the macrocycle ring plane, while for the Pro^5-Nle^6 an equilibrium should occur, the conformer with the H_N pointing up being the most populated (85%).

Previous MD simulations with time-dependent distance restraints have been shown to improve significantly the agreement between the calculated proton−proton distances and the experimentally derived distances.[32,42] In particular, in the case of the flip of the central peptide bond in cyclic hexapeptides, this method is able to reproduce fast conformational equilibrium on the NMR time scale. The data reported in the Table 2 for compounds **I** and **II**, indeed, show that the time-averaged simulations greatly improve the agreement between the experimentally derived distances and the calculated distances. Figure 5 shows the characteristic distances of the reverse turns, i.e., the $H_N(i + 2)-H_\alpha(i + 1)$ and $H_N(i + 2)-H_\alpha(i + 2)$, for both Pro^5-Nle^6 and Pro^2-Phe^3 segments in compounds **I** and **II**, along the time-averaged molecular dynamics. As is the case in a type I/type II equilibrium, better agreement is obtained by sampling the two conformations of the reverse turn, involving the flip of the peptide bond relative to the pseudopeptide ring plane.

Discussion

Tremendous amounts of data have been accumulated in the last 10 years on the conformational properties of the cyclic hexapeptides.[26,34,42,45] Extensive conformational analysis of these cyclic peptides has shown that these molecules adopt in general a "canonic" backbone conformation, a two-reverse-turn structure both in the solid state and in solution. However, more recently, several studies of the conformational properties of some cyclic peptides in solution, from NMR data, have provided evidence for the existence of conformational equilibrium in these molecules, which is fast on the NMR time scale.[32,34,41-43] Also, while it is difficult to evaluate the conformational homogeneity of a molecule in solution, there are some rules which, when fulfilled, could indicate the presence of a single highly favored conformation.[26,27,31] In this respect, a particular feature of these two molecules is the dispersion of several methylene proton chemical shifts, as well as the observation of a specific set of vicinal coupling constants, both at the level of the backbone and the side chains. Thus, the existence of a predominant conformation in these two cyclic peptides in aqueous solution can be proposed, at least for those molecules containing all trans peptide bonds. This proposal is supported by the internal consistency of the rOe data set, which leads to the determination of a major conformation containing very few distance restraint violations. Motions fast on the NMR time scale, which have been reported in many studies, involving the orientation of the central peptide

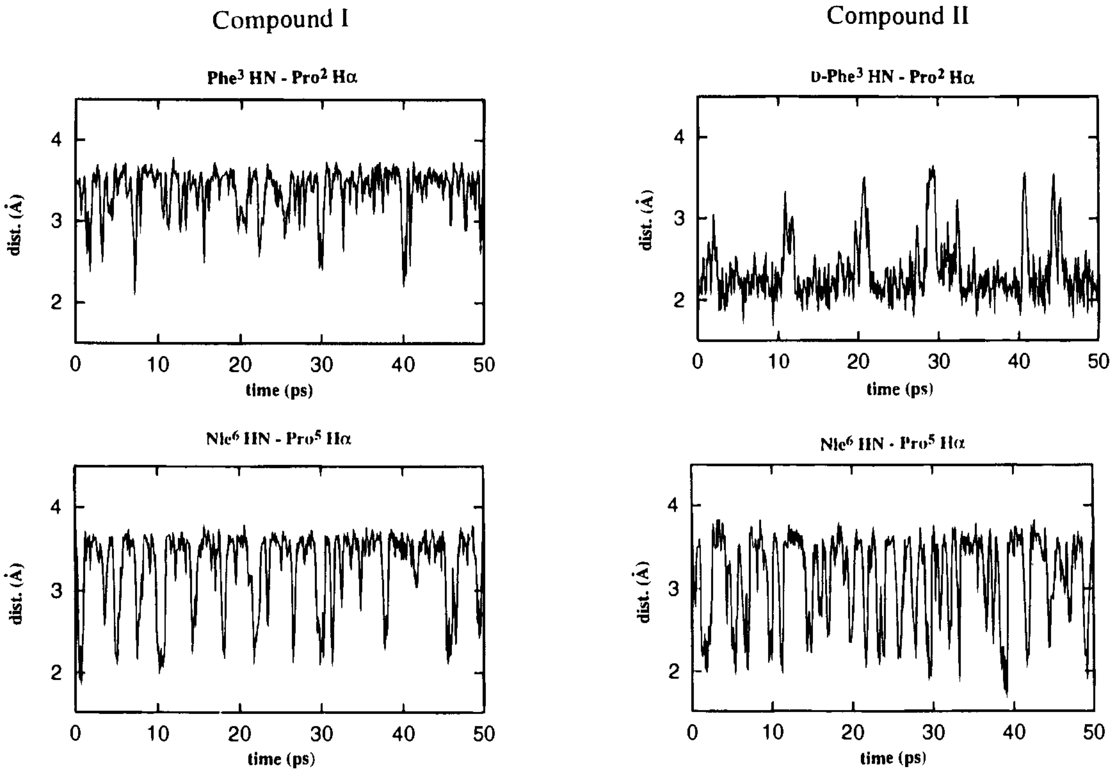

Figure 5. Interatomic distances as a function of time during the time-averaged molecular dynamics for compounds **I** and **II**. The assignment of each reported distance is given at the top of the corresponding plot.

bond of the β-turn,[32,41,42] have been also detected in these two molecules.

A striking feature in the 3D structure of these cyclic peptides is the orientation of the peptide bonds. As can be seen in Figures 3 and 4, the peptide bonds in these peptides have almost perpendicular orientation with respect to the plane formed by the peptide macrocycle. This orientation makes impossible the formation of any intramolecular hydrogen bonds in these peptides, as supported by the temperature coefficient measured for the H_N protons in these molecules. As mentioned above, such an orientation of the peptide bonds is a characteristic of the type VIII-turn. To our knowledge, this is the first report of the occurrence of a type VIII β-turn in a cyclic peptide. However, it should be noticed that in proteins the type VIII-turn is the most prevalent one after the two classic type I- and II-turns. Several hypotheses can be proposed to explain why this type VIII-turn has not been observed in the cyclic peptides. One possibility could be that, for solubility reasons, the solvent of choice for the NMR study of cyclic peptides is dimethyl sulfoxide. Due to the difference in the solvation properties of these two solvents, it might be possible that the type VIII-turns are stabilized by some preferential intermolecular interactions between the peptide and water. The perpendicular orientation of the peptide bonds should favor such interactions between water molecules and both the carbonyl and the amide groups. Furthermore, some hydrophobic packing between the Phe³/Pro² and Nle⁶/Pro⁵ side chains may stabilize this turn in water (the rOe effects observed between these side chains provide evidence of their spatial proximity). However, we cannot exclude that the presence of the phosphinic bond in these cyclic peptides participates to the stabilization of this particular turn. These different questions are currently under study in our laboratory by probing the role of the solvent as well as the importance of the different functional groups in these molecules.

The influence of Phe³ stereochemistry on Gly¹, a medium range distance effect, a priori unexpected, might tentatively be explained by looking at the 3D structure of these molecules, as determined by this study. While the global folding of the backbone in compound **I** is rather typical of a standard two-reverse-turn structure, in compound **II** the folding of the backbone around the phosphinic residue is extremely unusual, producing overall an asymetric macrocycle. This could limit the mobility of the backbone and thus restrict the occurrence of some motions around Gly¹. As shown in Figures 3 and 4, the hydroxyphosphinyl group points toward the outside of the peptide macrocycle. This particular orientation is probably imposed by the preferred ψ value of a phosphinic residue. In fact, in these two compounds, we have observed that the adopted ψ value places the two oxygen atoms in a gauche orientation relative to the C_γ atom of the phenyl side chain, the orientation of which being defined by the stereochemistry of the Phe³ residue.

The specific structure displayed by compounds **I** and **II** might be used to explain previous results for the activity of these cyclic compounds. While, the modifications of the stereochemistry of the P_1 (Phe³) residue in the linear phosphinic inhibitors of bacterial collagenase leads to a strong decrease of the potency (by a factor 18), surprisingly in the case of the cyclic peptides the same modification only produces a change of the potency by a factor less than 2. In addition to the different factors which have been discussed in a previous study to explain this observation,[19] the particular orientation of the hydrophosphinyl group found in compounds **I** and **II** should also be taken into consideration to rationalize the potency of these cyclic peptides. In fact, it can be seen from Figures 3 and 4 that if the hydroxyphosphinyl

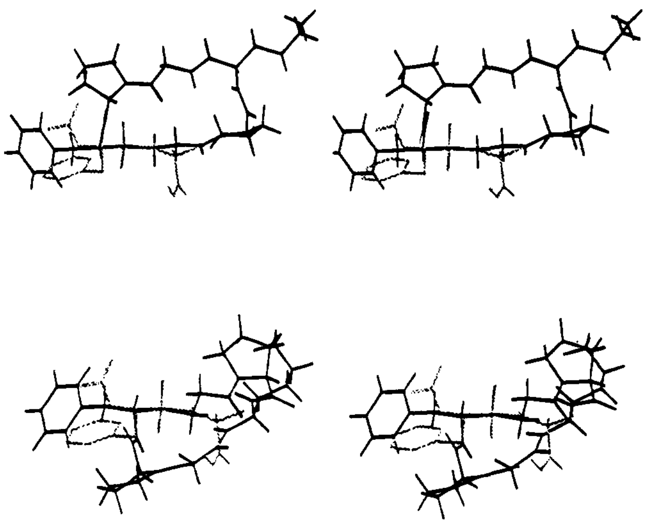

Figure 6. Superimposition of the phosphorus inhibitor of thermolysin[45] CBZ-Phe-ψ(PO_2-NH)-Leu-Ala on the structure of compound **I** (top) and **II** (bottom).

group in these molecules points toward the outside of the peptide macrocycle, their respective orientations with respect to this macrocycle are quite different. From this remark, it follows that apart the interactions of the hydroxyphosphinyl group of these molecules with the active site, which are assumed to be similar, the other parts of these cyclic peptides would interact with the active site of the collagenase in a very different manner. To illustrate this point, we tentatively superimpose the structure of a phosphorus–peptide inhibitor, bound to the active site of thermolysin,[46] on those of compounds **I** and **II**. Although there is no structural evidence for similarity between the 3D structure of the catalytic domain of thermolysin and bacterial collagenase, previous studies have shown that the spatial relationship between the zinc atom and the S_1 and S_1' subsites is rather conserved in the zinc metalloprotease family.[47] The structures of the thermolysin inhibitor and that of compounds **I** and **II** have been superimposed in order to obtain a good fit between the hydroxyphosphinyl groups of these molecules. The model presented in Figure 6 clearly highlights how the interaction of the hydroxyphosphinyl group of compounds **I** and **II**, with a putative zinc atom, would imply a very different relative orientation of the peptide macrocycle of these inhibitors, with respect to the collagenase active site in each case. Further, it can be seen that even if the fit between the phenyl side chain of the thermolysin inhibitor and those of compounds **I** and **II** is not perfect, their mean orientation is similar. Interestingly, from this comparison, it can be predicted that a leucine side chain, introduced in position 4 of the cyclic peptide, should occupy a location similar to that observed for the leucine side chain in the thermolysin inhibitor.

Conclusions

The determination of the 3D structures of these cyclic pseudopeptides in aqueous solution confirms previous predictions made on the overall structure of these inhibitors. In particular, this study demonstrates that the hydroxyphosphinyl group points effectively toward the outside of the peptide macrocycle, in an orientation compatible with a subsequent interaction of this group with the zinc atom of the enzyme active site. However, it should be stressed that neither the apparent rigidity of these cyclic peptides nor the specific conformation of compound **II** have been correctly anticipated. The precise knowledge of the 3D structures of these inhibitors would help us to design chemical modifications which can lock them in a conformation fitting best the protease active site. The development of very potent constrained cyclic pseudopeptide inhibitors of bacterial collagenases represents an interesting challenge, not only because such molecules may lead to a rational design of peptidomimetics as inhibitors of these enzymes[48,49] but also because, as discussed above, such a strategy might be extended to the design of other cyclic phosporus–peptides as inhibitors of other zinc metalloproteases, a field of great medicinal importance and in rapid expansion.

Experimental Section

NMR Measurements. NMR spectra of cyclo(Gly^1-Pro^2-Phe$^{3}\psi$[PO_2-CH_2]Gly^4-Pro^5-Nle^6) (compound **I**) and cyclo(Gly^1-Pro^2-D-Phe$^{3}\psi$[PO_2-CH_2]Gly^4-Pro^5-Nle^6) (compound **II**) were recorded on a Bruker AMX500 spectrometer. The sample concentration of I and II was 10 mM in 90% H_2O, 10% D_2O, pH 2.3. The NMR data were processed on a SGI indigo R4000 workstation with the Felix 2.1 software.[50] All spectra were recorded at 280 K except for the temperature coefficients which were measured for the amide resonance by varying the temperature from 280 to 303 K.

Chemical shifts were measured relative to internal reference sodium 2,2,3,3-tetradeuterio-3- (trimethylsilyl)propionate (TSP). All 2D NMR spectra were recorded with simultaneous detection in F2. Quadrature detection in F1 was achieved by time-proportional phase incrementation.[51] Water suppression was achieved by presaturation during the relaxation delay. TOCSY spectra[52,53] were recorded with either a 20 or 80 ms Waltz16 sequence for the isotropic mixing,[54] a 1 s relaxation delay, 64 scans, 2048 complex data points in F2, and 256 experiments in F1.

Coupling constants were determined either in the 1D resolution-enhanced spectrum, DQF-COSY spectrum,[55,56] or E-COSY spectrum.[57–59] The ϕ values were determined from the $^3J(H_N-H_\alpha)$ coupling constants using a Bystrov's–Karplus equation.[39] The populations of the three rotamers of the Nle side chains were determined from the $^3J(H_\alpha-H_\beta)$ coupling constants using Pachler's equation.[39,60,61] In the case of residue Phe, these population were estimated from the $^3J(H_\alpha-H_\beta)$ using a calibration of the ^3J_g and ^3J_t constants for phosphorus analogues.[33]

The assignment of the ^{13}C resonances was achieved by analysis of an inverse $^{13}C-^1H$ shift correlation (HMQC).[35,62] This makes it possible to determine the J_{C-P} coupling constant directly from analysis of the 1D $^{13}C-^1H$-decoupled spectrum of the cyclohexapeptides. The aromatic proton resonances were assigned using HMQC experiments in conjunction with heteronuclear long range correlation experiments (HMBC).[36] The HMBC experiments were recorded with a delay $\Delta 1$ of 3.3 ms, a delay $\Delta 2$ of 60 ms, 2048 complex data points in F2, and 256 experiments in F1. The spectral width in F1 (^{13}C) was 27 669 Hz. The ^{13}C decoupling during aquisition was achieved with a GARP sequence.

ROESY spectra[63] were recorded with 128 scans, a 2 s relaxation delay, 2048 complex data points in F2, and 256 experiments in F1. The spectral width in both dimensions was 6024 Hz. After zero filling, the final size of the matrix was 1024 × 1024. For integration, apodization with a sine bell function shifted by 90° was used in both dimensions. The mixing period was achieved by a repetitive sequence $(\beta - \tau)_n$.[64]

The distance restraints were determined from analysis of the buildup rate of the rOe in a series of five ROESY spectra recorded with mixing times of 85, 105, 125, 145, and 165 ms. After Fourier transform, all ROESY spectra were corrected using T1 noise reduction and/or local base plane correction routines written in the macrolanguage of the Felix software.

In each ROESY experiment, the volume of a cross-peak (i,j) was integrated. The volumes of the corresponding diagonal peaks were also measured to give a corrected intensity according to the procedure suggested by Macura et al.[65] and used by Kazmierski et al.[66] In the case where one of the diagonal peaks was not sufficiently resolved for integration, the cross-peak was scaled with respect to one of them. As the nOe's observed at 500 MHz were very weak, no offset correction was applied.

rOe buildup rates were estimated using least squares fitting of the five measured points. Only the buildup rates for which the linear fit gave a correlation coefficient greater than 0.9 were used to calculate distance restraints.

The r_{ij} distances were calculated using the well-known relation:

$$r_{ij} = r_{\text{ref}}\sqrt[6]{\frac{\sigma_{ij}}{\sigma_{\text{ref}}}}$$

where r_{ref}, r_{ij}, σ_{ref}, and σ_{ij} refer respectively to the interproton distance and to the slope of the intensity of the cross-peak versus the mixing time for the reference pair and for the pair for which the distance is unknown.

The "soft" ROESY experiment was recorded using a sequence adapted from the z-ROESY sequence.[67] The F1 and F2 dimensions were restricted by selective exitation through a DANTE-Z train[68] applied to the Gly[1], Nle[6] H_N region, as already reported for a "soft" z-TOCSY experiment.[69] The spectral width in F1 and F2 was 250 Hz; 512 complex data points were recorded in the F2 dimension; 128 experiments in the F1 dimension were recorded in the RuSH methods[70] in order to achieve quadrature detection.

Conformation Searches. Structures compatible with the experimental distance restraints obtained as described above have been generated by a procedure of simulated annealing[71] with the X-PLOR software.[72,73] The distance restraints, when used, were incorporated in the total energy potential using a square well function.[73] In order to take into account the uncertainty in the distances obtained as describded above, lower and upper bounds calculated from r_{ij} − 20% and r_{ij} + 20%, respectively, were used in the following steps of this work.

Starting from random positions of the atoms of the molecule, initial structures were subjected to 100 steps of minimization in the distance geometry force field of X-PLOR v 3.1 (parmallhdg), the potential energy containing only the bond, angle, and van der Waals terms. A second 100- step minimization was carried out, the potential energy function containing the same terms as for the first initial minimization plus the improper dihedral, and distance restraint terms (k_{DR} = 1 kcal mol^{-1} A^{-2}). A 2.5 ps molecular dynamics was then carried out. During this step, the temperature was maintained at 1000 K by strong coupling to a temperature bath.[74] The resulting structures were submitted to 500 steps of energy minimization followed by a 45 ps simulated annealing from 1000 K to 100 K in the parmallhdg force field of X-PLOR v 3.1, the potential energy function containing the bond, angle, van der Waals, dihedral, improper, and distance restraints terms. During this step the distance restraints constant (k_{DR}) was regularly increased from 1 to 50 kcal mol^{-1} A^{-2}. The simulated annealing step was followed by a final minimization in the parmallhdg force field of X-PLOR v 3.1. The resulting structures were finally minimized in the CHARMM force field[75] version 22 of the XPLOR v 3.1 software with Lennard Jones potential for van der Waals interactions and a CDIE treatment of the electrostatic interactions (ϵ = 80). All calculations were carried out in vacuo. Only structures having a total energy violation limited to 10 kcal/mol above the lowest total energy and a distance restraints energy limited to 1.5 kcal/mol were saved. It should be noticed that in practice no structure having a total energy 2.5 kcal/mol above the lowest total energy and a distance restraints energy 0.5 kcal/mol above the lowest distance restraints energy was found.

Time-dependent distance restraints molecular dynamics[76,77] was carried out in the CHARMM 22 force field of the XPLOR v 3.1. This procedure requires that the distance restraints are satisfied as a $\langle r^{-3}\rangle - {}^1/_3$ time-weighted average over the simulated trajectory. The time constant for the exponential decay of the memory function was set to 2.5 ps. A 10 ps molecular dynamics without time-dependent restraints was used to equilibrate the structure before running the 50 ps time-dependent distance restraints molecular dynamics. The distance restraints constant (k_{DR}) was set to 5 kcal mol $^{-1}$ Å^{-2}. The parameters used to define the geometry and the charges of the phosphinic group were taken from Merz and Kollman.[78]

Acknowledgment. We wish to thank Dr. Roumestand for the "soft" ROESY experiment and Dr. Gilquin for assistance in the use of the XPLOR software.

References

(1) Murphy, G. J. P.; Murphy, G.; Reynolds, J. J. The Origin of Matrix Metalloproteinases and their Familial Relationships. *FEBS Lett.* **1991**, *289*, 4−7.

(2) Schiavo, G.; Poulain, B.; Rossetto, O.; Benfenati, F.; Tauc, L.; Montecucco, C. Tetanus Toxin is a Zinc Protein and its Inhibition of Neurotransmitter Release and Protease Activity Depend on Zinc. *EMBO J.* **1992**, *11*, 3577−3583.

(3) Schiavo, G.; Rossetto, O.; Santucci, A.; DasGupta, B. R.; Montecucco, C. Botulinum Neurotoxins are Zinc Proteins. *J. Biol. Chem.* **1992**, *267*, 23479−23483.

(4) Häse, C. C.; Finkelstein, R. A. Bacterial Extracellular Zinc-containing Metalloproteases. *Microbiol. Rev.* **1993**, *57*, 823−837.

(5) Jiang, W.; Bond, J. S. Families of metalloendopeptidases and their relationships. *FEBS Lett.* **1992**, *312*, 110−114.

(6) Dumermuth, E.; Sterchi, E. E.; Jiang, W.; Wolz, R. L.; Bond, J. S.; Flannery, A. V.; Beynon, R. J. The Astacin Family of Metalloendopeptidases. *J. Biol. Chem.* **1991**, *266*, 21381−21385.

(7) Bode, W.; Gomis-Rüth, F. X.; Huber, R.; Zwilling, R.; Stöcker, W. Structure of Astacin and Implications for Activation of Astacins and Zinc-ligation of Collagenases. *Nature* **1992**, *358*, 164−166.

(8) Gomis-Rüth, F. X.; Kress, L. F.; Bode, W. First Structure of a Snake Venom Metalloproteinase: a Prototype for Matrix Metalloproteinases / Collagenases. *EMBO J.* **1993**, *12*, 4151−4157.

(9) Bode, W.; Gomis-Rüth, F. X.; Stöcker, W. Astacins, Serralysins, Snake Venom and Matrix Metalloproteinases Exhibit Identical Zinc-binding Environments (HEXXHXXGXXH and Met-turn) and Topologies and Should Be Grouped into a Common Family, the 'Metzincins'. *FEBS Lett.* **1993**, *331*, 134−140.

(10) Bode, W.; Reinemer, P.; Huber, R.; Kleine, T.; Schnierer, S.; Tschesche, H. The X-Ray Crystal Structure of the Catalytic Domain of Human Neutrophil Collagenase Inhibited by a Substrate Analogue Reveals the Essentials for Catalysis and Specificity. *EMBO J.* **1994**, *13*, 1263−1269.

(11) Gomis-Rüth, F. X.; Stöcker, W.; Huber, R.; Zwilling, R.; Bode, W. Refined 1.8 Å X-Ray Crystal Structure of Astacin, a Zinc-endopeptidase from the Crayfish *Astacus astacus L. J. Mol. Biol.* **1993**, *229*, 945−968.

(12) Gomis-Rüth, F. X.; Kress, L. F.; Kellerman, J.; Mayr, I.; Lee, X.; Huber, R.; Bode, W. Refined 2.0 Å X-Ray Crystal Structure of the Snake Venom Zinc-endopeptidase Adamalysin II. *J. Mol. Biol.* **1994**, *239*, 513−544.

(13) Netzel-Arnett, S.; Sang, Q.-X.; Moore, W. G. I.; Navre, M.; Birkedal-Hansen, H.; Van Wart, H. E. Comparative Sequence Specificities of Human 72-and 92-kDa Gelatinases (Type IV Collagenases) and PUMP (Matrilysin). *Biochemistry* **1993**, *32*, 6427−6432.

(14) Grobelny, D.; Poncz, L.; Galardy, R. E. Inhibition of Human Skin Fibroblast Collagenase, Thermolysin and *Pseudomonas aeruginosa* Elastase by Hydroxomic Acid. *Biochemistry* **1992**, *31*, 7152−7154.

(15) Chapman, K. T.; Kopka, I. E.; Durette, P. L.; Esser, C. K.; Lanza, T. J.; Izquierdo-Martin, M.; Niedzwiecki, L.; Chang, B.; Harrison, R. K.; Kuo, D. W.; Lin, T. Y.; Stein, R. L.; Haymann, W. K. Inhibition of Matrix Metalloproteinases by N-carboxyalkyl Peptides. *J. Med. Chem.* **1993**, *36*, 4293−4301.

(16) Brown, F. K.; Brown, P. J.; Bickett, D. M.; Chambers, C. L.; Davies, H. G.; Deaton, D. N.; Drewry, D.; Foley, M.; Mc Elroy, A. B.; Creyson, M.; Mc Greeham, G. M.; Myers, P. L.; Norton, D.; Salovich, J. M.; Schoenen, F. J.; Ward, P. Matrix metalloproteinases Inhibitors Containing a (Carboxyalkyl) Amino Zinc Ligand: Modification of the P1 and P2′ residues. *J. Med. Chem.* **1994**, *37*, 674−688.

(17) Morgan, B. P.; Scholtz, J. M.; Ballinger, M. D.; Zipkin, I. D.; Bartlett, P. A. Differential Binding Energy: A Detailed Evaluation of the Influence of Hydrogen-Bonding and Hydrophobic Groups on the Inhibition of Thermolysin by Phosphorus-Containing Inhibitors. *J. Am. Chem. Soc.* **1991**, *113*, 297−307.

(18) Yiotakis, A.; Lecoq, A.; Nicolaou, A.; Labadie, J.; Dive, V. Phosphinic Peptide Analogues as Potent Inhibitors of *Corynebacterium rathayii* Bacterial Collagenase. *Biochem. J.* **1994**, *303*, 323−327.

(19) Yiotakis, A.; Lecoq, A.; Vassiliou, S.; Raynal, I.; Cuniasse, P.; Dive, V. Cyclic peptides with a Phosphinic Bond as Potent Inhibitors of a Zinc Bacterial Collagenase. *J. Med. Chem.* **1994**, *37*, 2713–2720.
(20) Kessler, H.; Anders, U.; Schudok, M. An Expected Cis Peptide bond in the Minor Conformation of a Cyclic Hexapeptide Containing Only Secondary Amide Bonds. *J. Am. Chem. Soc.* **1990**, *112*, 5908–5916.
(21) Bairaktari, E.; Mierke, D. F.; Mammi, S.; Peggion, E. Observation of a Cis Amide Isomer within a Linear Peptide. *J. Am. Chem. Soc.* **1990**, *112*, 5383.
(22) Mierke, D. F.; Yamazaki, T.; Said-Nejad, O. E.; Felder, E. R.; Goodman, M. Cis/Trans Isomers in Cyclic Peptides without N-Substituted Amides. *J. Am. Chem. Soc.* **1989**, *111*, 6847–6849.
(23) Dorman, D. E.; Bovey, F. A. Carbon 13 Magnetic Resonance Spectroscopy. The Spectrum of Proline in Oligopeptides. *J. Org. Chem.* **1973**, *38*, 2379–2383.
(24) Deber, C. M.; Madison, V.; Blout, E. R. Why Cyclic Peptides? Complementary Approaches to conformations. *Acc. Chem. Res.* **1976**, *9*, 106–113.
(25) Gierash, L. M.; Karle, I. L.; Rockwell, A. L.; Yenal, K. Crystal and Solution Structure of *cyclo*(Ala-Pro-Gly-D-Phe-Pro): A New Type of cyclic pentapeptide which Undergoes Cis-Trans Isomerization of the Ala-Pro Bond. *J. Am. Chem. Soc.* **1985**, *107*, 3321–3327.
(26) Kessler, H. Conformation and Biological Activity of Cyclic Peptides. *Angew. Chem., Int. Ed. Engl.* **1982**, *21*, 512–523.
(27) Kopple, K. D.; Wang, Y.; Cheng, A. G.; Bhandary, K. K. Conformations of Cyclic Octapeptides. 5. Crystal Structure of Cyclo(Cys-Gly-Pro-Phe)$_2$ and Rotating Frame Relaxation ($T_{1\rho}$) NMR Studies of Internal Mobility in Cyclic Octapeptides. *J. Am. Chem. Soc.* **1988**, *110*, 4168–4176.
(28) Kessler, H.; Hehlein, W.; Schuck, R. Peptide Conformation 15. One- and Two-Dimensional ^{1}H, ^{13}C, and ^{15}N NMR Studies of cyclo(Pro-Phe-Gly-Phe-Gly)$_n$ (n=1, 2): Selective Complexation of Lithium Ions (n=1) and Potassium Ions (n=2). *J. Am. Chem. Soc.* **1982**, *104*, 4534–4540.
(29) Hruby, V. J.; Kao, L.-F.; Pettitt, B. M.; Karplus, M. The Conformational Properties of the Delta Opioid Peptide [D-Pen2, D-Pen5]enkephalin in Aqueous Solution Determined by NMR and Energy Minimization Calculations. *J. Am. Chem. Soc.* **1988**, *110*, 3351–3359.
(30) Rose, G. D.; Gierasch, L. M.; Smith, J. A. Turns in Peptides and Proteins. *Adv. Protein Chem.* **1985**, *37*, 1–109.
(31) Kessler, H.; Bats, J. W.; Griesinger, C.; Koll, S.; Will, M.; Wagner, K. Peptide Conformations. 46. Conformational Analysis of a Superpotent Cytoprotective Cyclic Somatostatin Analogue. K. *J. Am. Chem. Soc.* **1988**, *110*, 1033–1049.
(32) Kessler, H.; Matter, H.; Gemmecker, G.; Kottenhahn, M.; Bats, J. W. Structure and Dynamics of a Synthetic O-Glycosylated Cyclopeptide in Solution Determined by NMR Spectroscopy and MD Calculations. *J. Am. Chem. Soc.* **1992**, *114*, 4805–4818.
(33) Siatecki, Z.; Kozlowski, H. ^{1}H and ^{31}P NMR Studies of Rotational Isomerism in Phosphorus Analogs of Aspartic Acid, 3-Amino-3-Phosphonatopropionic and 3-Amino-3-(Methylphosphinato) Propionic Acids. *Org. Magn. Reson.* **1981**, *17*, 172–174.
(34) Bean, J. W.; Kopple, K. D.; Peishoff, C. E. Conformational Analysis of Cyclic Hexapeptides Containing the D-Pro-L-Pro Sequence To Fix β-Turn Position. *J. Am. Chem. Soc.* **1992**, *114*, 5328–5334.
(35) Müller, L. Sensitivity Enhanced Detection of Weak Nuclei Using HeteroNuclear Multiple Quantum Coherence. *J. Am. Chem. Soc.* **1979**, *101*, 4481–4484.
(36) Bax, A.; Summers, M. F. 1H and 13C Assignments from Sensitivity-Enhanced Detection of Heteronuclear Multiple-Bond Connectivity by 2D Multiple Quantum NMR. *J. Am. Chem. Soc.* **1986**, *108*, 2093–2094.
(37) Wilmot, C. M.; Thornton, J. M. β-Turns and Their Distorsions: a Proposed New Nomenclature. *Protein Eng.* **1990**, *3*, 479–493.
(38) De Marco, A.; Llinas, M.; Wüthrich, K. Analysis of the 1H-NMR Spectra of Ferrichrome Peptides. I. The non Amide Protons. *Biopolymers* **1978**, *17*, 637–650.
(39) Bystrov, V. F. Spin-Spin Coupling and the Conformational States of Peptide Systems. *Prog. NMR Spectrosc.* **1976**, *10*, 41–81.
(40) Lankhorst, P. P.; Haasnoot, C. A. G.; Erkelens, C.; Altona, C. Carbon 13 NMR in Conformational Analysis of Nucleic Acid Fragments 2. A Reparametrization of the Karplus Equation for Vicinal NMR Coupling Constants in CCOP and HCOP Fragments. *J. Biomol. Struct. Dyn.* **1984**, *1*, 1387–1405.
(41) Stradley, S. J.; Rizo, J.; Bruch, M. D.; Stroup, A. N.; Gierash, L. M. Cyclic Pentapeptides as Models for Reverse Turns: Determination of the equilibrium Distribution Between Type I and Type II Conformations of Pro-Asn ans Pro-Ala β-Turns. *Biopolymers* **1990**, *29*, 263–287.
(42) Kessler, H.; Matter, H.; Gemmecker, G.; Kling, A.; Kottenhahn, M. Solution Structure of a Synthetic N-Glycosylated Cyclic Hexapeptide by NMR spectroscopy and MD Calculations. *J. Am. Chem. Soc.* **1991**, *113*, 7550–7563.
(43) Kopple, K. D.; Bean, J. W.; Bhandary, K. K.; Brian, J.; D'Ambrosio, C. A.; Peishoff, C. E. Conformationnal Mobility in Cyclic Oligopeptides. *Biopolymers* **1993**, *33*, 1093–1099.
(44) Narasinga Rao, B. N.; Kumar, A.; Balaram, H.; Ravi, A.; Balaram, P. Nuclear Overhauser Effects and Circular Dichroism as Probes of β-Turn Conformations in Acyclic and Cyclic Peptides with Pro-X Sequences. *J. Am. Chem. Soc.* **1983**, *105*, 7423–7428.
(45) Yang, C.-H.; Brown, J. N.; Kopple, K. D. Crystal Structure and Solution Studies of the Molecular Conformation of the Cyclic Hexapeptide cyclo-(Gly-L-His-L-Ala-L-Tyr-Gly). *J. Am. Chem. Soc.* **1981**, *103*, 1715–1719.
(46) Holden, H. M.; Tronrud, D. E.; Monzingo, A. F.; Weaver, L. H.; Mathews, B. W. Slow- and Fast- Binding inhibitors of Thermolysine Display Different Modes Binding. Crystallographic Analysis of Extended Phosphonamidate Transition State Analogues. *Biochemistry* **1987**, *26*, 8542–8553.
(47) Lovejoy, B.; Cleasby, A.; Hassel, A. M.; Longley, K.; Luther, M. A.; Weigl, D.; McGeehan, G.; McElroy, A. B.; Drewry, D.; Lambert, M. H.; Jordan, S. R. Structure of the Catalytic Domain of Fibroblast Collagenase Complexed with an Inhibitor. *Science* **1994**, *263*, 375–377.
(48) Marshall, G. R. A Hierarchical approach to peptidomimetic design. *Tetrahedron* **1993**, *49*, 3547–3558.
(49) Olson, G. L.; Bolin, D. R.; Pat Bonner, M.; Bös, M.; Cook, C. M.; Fry, D. G.; Graves, B. J.; Hatada, M.; Hill, D. E.; Khan, M.; Madison, V. S.; Rusiecki, V. K.; Sarabu, R.; Sepinwall, J.; Vincent, G. P.; Voss, M. E. Concepts and progress in the development of peptide mimetics. J. Med. Chem. **1993**, *36*, 3039–3049.
(50) Biosym Technologies Inc., 10065 Barnes Canyon Rd., San Diego, CA 92121.
(51) Marion, D.; Wüthrich, K. Application of Phase-sensitive Two-Dimensional Correlated Spectroscopy (COSY) for Measurements of ^{1}H-^{1}H Spin-Spin Coupling Constants in Proteins. Biochem. Biophys. Res. Commun. **1983**, *113*, 967–974.
(52) Braunschweiler, L.; Ernst, R. R. Coherence Transfer by Isotropic Mixing: Application to Proton Correlation Spectroscopy. J. Magn. Reson. **1983**, 53, 521–528.
(53) Davis, D. G.; Bax, A. Assignment of Complex ^{1}H- NMR Spectra with Two-Dimensional Homonuclear Hartmann-Hahn Spectroscopy. J. Am. Chem. Soc. **1985**, *107*, 2820–2821.
(54) Shaka, A. J.; Keeler, J. K.; Freeman, R. Evaluation of a New Broadband Decoupling Sequence: WALTZ-16. *J. Magn. Reson.* **1983**, *53*, 313–340.
(55) Piantini, U.; SØrensen, O. W.; Ernst, R. R. Multiple Quantum Filters for Elucidating NMR Coupling Networks. *J. Am. Chem. Soc.* **1982**, *104*, 6800–6801.
(56) Rance, M.; SØrensen, O. W.; Bodenhausen, G.; Wagner, G.; Ernst, R. R.; Wüthrich, K. Improved Spectral Resolution in COSY ^{1}H NMR Spectra of Proteins via Double Quantum Filtering. *Biochem. Biophys. Res. Commun.* **1983**, *117*, 479–485.
(57) Griesinger, C.; SØrensen, O. W.; Ernst, R. R. Two Dimensional Correlation of Connected NMR transitions. *J. Am. Chem. Soc.* **1985**, *107*, 6394–6397.
(58) Griesinger, C.; SØrensen, O. W.; Ernst, R. R. Correlation of Connected Transition by Two Dimensional NMR Spectroscopy. *J. Chem. Phys.* **1986**, *85*, 6837–6852.
(59) Griesinger, C.; SØrensen, O. W.; Ernst, R. R. Practical Aspects of the E. COSY technique. Measurement of Scalar Spin-Spin Coupling Constants in Peptides. *J. Magn. Reson.* **1987**, *75*, 474–492.
(60) Pachler, K. G. R. Extended Hückel Theory MO Calculation of Proton-Proton Coupling Constants - II. The Effect of Substituents on Vicinal Coupling in Monosubstituted Ethanes. *Tetrahedron* **1971**, *27*, 187–199.
(61) Pachler, K. G. R. The dependance of Vicinal Proton-Proton Coupling Constants on Dihedral Angle and Substituents *J. Chem. Soc., Perkin Trans. II* **1972**, 1936–1940.
(62) Bax, A.; Griffey, R. H.; Hawkins, L. B. Correlation of Proton and Nitrogen-15 Chemical Shifts by Multiple Quantum NMR. *J. Magn. Reson.* **1983**, *55*, 301–315.
(63) Bothner-By, A. A.; Stephens, R. L.; Lee, J.; Warren, C. D.; Jeanloz, R. W. Structure Determination of a Tetrasaccharide: Transient Nuclear Overhauser Effects in the Rotating Frame. *J. Am. Chem. Soc.* **1984**, *106*, 811–813.
(64) Kessler, H.; Griesinger, C.; Kerrsebaum, R.; Wagner, K.; Ernst, R. R. Separation of Cross-Relaxation and J Cross-Peaks in 2D Rotating-Frame NMR Spectroscopy. *J. Am. Chem Soc.* **1987**, *109*, 607–609.
(65) Macura, S.; Farmer, B. T.; Brown, L. R. An Improved Method for the Determination of Cross-Relaxation Rates from NOE Data. *J. Magn. Reson.* **1986**, *70*, 493–499.
(66) Kazmierski, W. M.; Yamamura, H. I.; Hruby, V. Topographic Design of Peptide Neurotransmitters and Hormones on Stable Backbone Templates: Relation of Conformation and Dynamics to Bioactivity. *J. Am. Chem. Soc.* **1991**, *113*, 2275–2283.
(67) Rance, M. Improved Techniques for Homonuclear Rotating Frame and Isotropic Mixing Experiments. *J. Magn. Reson.* **1987**, *74*, 557–564.

(68) Boudot, D.; Canet, D.; Brondeau, J.; Boubel, J.-C. DANTE-Z, A New Approach for Accurate Frequency Selectivity Using Hard Pulses. *J. Magn. Reson.* **1989**, *83*, 428–439.
(69) Roumestand, C.; Canet, D.; Mahieu, N.; Toma, F. DANTE-Z, An Alternative to Low-Power Soft Pulses. Improvement of the Selection Scheme and Applications to Multidimensional NMR Studies of Proteins. *J. Magn. Reson.* **1994**, *106*, 168–181.
(70) States, D. J.; Haberkorn, R. A.; Ruben, D. J. A Two-Dimensional Nuclear Overhauser Experiment with Pure Absorption Phase in Four Quadrants. *J. Magn. Reson.* **1982**, *48*, 286–292.
(71) Nilges, M.; Clore, M.; Gronenborn, A. M. Determination of Three-Dimensional Structures of Proteins from Interproton Distance Data by Dynamical Simulated Annealing from a Random Array of Atoms. Circumventing Problems Associated with Folding. *FEBS Lett.* **1988**, *239*, 129–136.
(72) Brünger, A. T.; Kuriyan, J.; Karplus, M. Crystallographic R Factor Refinement by Molecular Dynamics. *Science* **1987**, *235*, 458–460.
(73) Brünger, A. T. X-PLOR version 3.1; Yale University Press: New Haven, London, 1992.
(74) Berendsen, H. J. C.; Potsma, J. P. M.; van Gunsteren, W. F.; DiNola, A.; Haak, J. R. Molecular Dynamics with Coupling to an External Bath. *J. Chem. Phys.* **1984**, *81*, 3684–3690.
(75) Brooks, B. R.; Bruccoleri, R. E.; Olafson, B. D.; States, D. J.; Swaminathan, S.; Karplus, M. CHARMM: A Program for Macromolecular Energy, Minimization and Dynamics Calculations. *J. Comput. Chem.* **1983**, *4*, 187–217.
(76) Torda, A. E.; Scheek, R. M.; van Gunsteren, W. F. Time-Dependent Distance Restraints in Molecular Dynamics Simulations. *Chem. Phys. Lett.* **1989**, *157*, 289–294.
(77) Torda, A. E.; Scheek, R. M.; van Gunsteren, W. F. Time-averaged Nuclear Overhauser Effect Distance Restraints Applied to Tendamistat. *J. Mol. Biol.* **1990**, *214*, 223–235.
(78) Merz, K. M.; Kollman, P. A. Free Energy Perturbation Simulations of the Inhibition of Thermolysin: Prediction of the Free Energy of Binding of a New Inhibitor. *J. Am. Chem. Soc.* **1989**, *111*, 5649–5658.

JM940632U